Author/s:
Maitra, S;Tian, Y;Cassidy, MJ

Title:
Investigation of the installation process of drag-in plate anchors from LDFE modelling

Date:
2022-11-04

Citation:
Maitra, S., Tian, Y. & Cassidy, M. J. (2022). Investigation of the installation process of drag-in plate anchors from LDFE modelling. Geotechnique, 74 (12), pp.1215-1227. https://doi.org/10.1680/jgeot.21.00402.

Persistent Link:
https://hdl.handle.net/11343/321977

Investigation of the installation process of drag-in plate anchors from LDFE modelling

Shubhrajit MAITRA
Research Fellow
Department of Infrastructure Engineering, Faculty of Engineering and Information Technology
The University of Melbourne
Victoria 3010, Australia.
Email: shubhrajit.maitra@unimelb.edu.au

Yinghui TIAN (corresponding author)
Associate Professor
Department of Infrastructure Engineering, Faculty of Engineering and Information Technology
The University of Melbourne
Victoria 3010, Australia.
Email: yinghui.tian@unimelb.edu.au

Mark J CASSIDY
Professor
Department of Infrastructure Engineering, Faculty of Engineering and Information Technology
The University of Melbourne
Victoria 3010, Australia.
Email: mark.cassidy@unimelb.edu.au

No. of words: 5485	(Text main body, appendices, acknowledgement)
No. of tables: 4	(671 words in tables including captions and notes)
No. of figures: 14	(27 figure parts in total)
No. of items in notation: 45	
No. of equations: 6	
No. of references: 47	

Investigation of the installation process of drag-in plate anchors from LDFE modelling

Shubhrajit Maitra, Yinghui Tian and Mark J Cassidy

Abstract

The installation of drag-in plate anchors is investigated using advanced large deformation finite element (LDFE) analysis. A new modelling technique that can realise the continuously evolving loading angle on the anchor line is described. The entire anchor trajectory is simulated till the anchor reached an ultimate state after dragging by a very large distance, typically in the range of 40 to 70 times of anchor width. An installation in simple uniform and non-sensitive soil is first presented with agreement against well-established plasticity and analytical solution offering verification of the techniques developed. The effects of anchor padeye position, seabed soil conditions, anchor line properties and anchor-soil interface on the installation response are then discussed. The findings highlight that plasticity and analytical approaches are not necessarily conservative when the yield surface derived from deep embedded anchors is applied in shallow conditions. The LDFE results also demonstrate the importance of accounting for soil remoulding around both the anchor and anchor installation line. The results of this study present insights for offshore engineers to consider and incorporate when estimating drag anchor installation trajectory and holding capacity.

Keywords: Anchors, Anchors & anchorages, Clays, Finite-element modelling, Offshore engineering

1. Introduction

With low installation costs, high holding efficiency and ability to be reused, drag anchors are an attractive option to secure the next generation of offshore facilities, such as floating wind turbines. The traditional fluke anchors, consisting of a main plate (termed a "fluke") and a shank, and the more recent vertically loaded anchors (VLAs) (see Fig. 1) are two typical forms of drag anchors (Dean, 2010; Randolph & Gourvenec, 2011). The fluke anchor is equipped with a fixed angle shank, whereas the modern VLA has a slim and adjustable shank to optimise the orientation and thus the holding capacity after installation.

Once deployed on the seabed, drag anchors are installed by pulling an installation line from an anchor handling vessel. The vessel's forward motion causes tension of the line and leads the anchor to embed. The anchor also rotates until the line tensile force passes through the rotation centre of the anchor (see Tian et al., 2018, 2020 for details). Consequently, rotation of the anchor stops, and in this ultimate state the anchor does not penetrate further deeper. Modelling this installation is extremely challenging, as the trajectory is difficult to visualise in soil during physical experiments, and large deformations are inevitably involved in numerical modelling.

The currently available predictions of drag anchor installation and trajectory can be classified into three categories: (a) empirical design charts (NCEL, 1987; API, 2005; Vryhof, 2018), (b) analytical methods based on force equilibrium or force-resultant plasticity models (Neubecker & Randolph, 1996; O'Neill et al., 2003; Murff et al., 2005; Aubeny & Chi, 2010; Cassidy et al., 2012; Wang et al., 2014; Tian et al., 2015a), and (c) advanced numerical modelling (Zhao & Liu, 2016; Dou & Yu, 2018). As summarised in Table 1, the empirical methods, expressed as design charts, simplistically relate the holding capacity and penetration depth as functions of anchor weight, soil shear strength and anchor type. The analytical methods are simple and easy to use (with most written as spreadsheets or computer software that takes seconds to run, see Cassidy et al., 2012), but they do not yet account for remoulding of soil around the anchor. As shown later in this paper, this can significantly overestimate the penetration depth and holding capacity. Because of the difficulties in large deformation analysis, limited numerical simulation of drag anchor installation can be found in the literature. There are some studies in related fields that have examined the "keying" process of suction embedded plate anchors and installation of dynamically embedded plate anchors (Song et al., 2009; Yu et al., 2009; Wang et al., 2011; Tian et al., 2015b; Chen et al., 2015; Ghorai & Chatterjee, 2021).

The installation of drag anchors involves extremely large deformations with drag distances approximately 5–10 times that of the ultimate penetration depth (DNV, 2012). This requires an efficient and rigorous large deformation finite element (LDFE) modelling. Sequential limit analysis using adaptive remeshing can be an alternative way to simulate such large deformation problems as it can accomplish accurate geometric updating with larger displacement increments, and thus be more efficient (Kong et al., 2017).

In this paper, the "remeshing and interpolation technique using small strain" (RITSS) technique (Hu & Randolph, 1998) is utilised to simulate the installation of drag anchors. RITSS has been proven robust and accurate in many applications, especially in offshore geotechnics (Wang et al., 2010, 2015; Chatterjee et al., 2012; Tian et al., 2014a, Ullah et al., 2018). The large deformation process is divided into a sequence of small incremental displacement steps of Lagrangian analysis. After each step, a new mesh is reconstructed based on the deformed domain obtained from the previous analysis, which eliminates mesh distortions that would otherwise occur. The stresses, strains and field variables are interpolated from the old mesh to the reconstructed mesh before carrying out the next increment analysis. By implementing in software Abaqus (Dassault Systèmes, 2013), the entire RITSS process is controlled using Python scripts (for remeshing and carrying out subsequent Lagrangian analyses) and Fortran subroutines (for interpolation of stresses, strains and field variables). A detailed demonstration of the RITSS methodology implemented and followed can be found in Chatterjee et al. (2012), Tian et al. (2014a) and Maitra et al. (2019) and for brevity is omitted here.

After verifying the numerical model against the established methodology of plasticity analysis and analytical solution, the installation process was examined by carrying out a parametric study of 17 LDFE analysis cases (each consuming an average running time of 96 hours on a workstation with Intel Core i7 processor, 2.8 GHz CPU, 32 GB memory, 4 cores, 8 threads). Evolution of the anchor line profile during installation has been incorporated by solving the governing differential equations of the anchor line (described in Section 2.3). The influence of anchor padeye position, soil strength gradient, soil remoulding and various anchor and line properties on drag anchor trajectory and holding capacity are explored.

2. Numerical methodology

2.1 Model setup

This study adopted a simplified rectangular plate geometry considering a fluke width of 3.41 m, a fluke length of 3.3 m and a shank length of 6.24 m. The bearing area (≈ 11.25 m^2) and shank length for the chosen plate is similar to that of a Vryhof Stevpris 10t Mk5 anchor (Vryhof, 2018). Modelling a complex three-dimensional (3D) anchor using LDFE technique requires significant computation time and remains computationally prohibitive for the multiple analyses required to explore generic anchor installation behaviour. As demonstrated by Wei et al. (2015) and Tian et al. (2018), the soil resistance to a 3D anchor can be represented by a two-dimensional anchor with a proper 'equivalent' thickness. In this paper, the anchor is simplified as a two-dimensional rectangular rigid body (see Fig. 2), wherein the equivalent thickness of the fluke t is taken as 0.51 m and thus results in an aspect ratio of $B/t \approx 7$, which has been widely adopted in the literature to represent a drag anchor (O'Neill et al., 2003; Murff et al., 2005; Yang et al., 2010). Fig. 2 illustrates the geometry and notations used. Murff et al. (2005) showed that the shank only contributes up to 10% of the total anchor resistance and therefore only the fluke was modelled for simplicity. Vryhof (2018) recommends three values of fluke-shank angle θ_{fs}: 50°, 41° and 32° for installation in soft, medium and stiff clays, respectively (see Figs 1–2 for illustration). All three cases of θ_{fs} were considered, which correspond to padeye offset ratios (proposed by Tian et al., 2014b, 2015a) $\eta = e_{\mathrm{p}}/e_{\mathrm{n}}$ of 0.48, 0.73 and 1.08, respectively, where e_{p} and e_{n} are the padeye offset and eccentricity, respectively, as defined in Fig. 2.

The shank initially aligns horizontally on the seabed prior to installation, and the fluke is inclined at an angle θ_{fs} to the horizontal, where this assumption of initial position agrees with previous studies (e.g. Neubecker & Randolph, 1996). The anchor was assumed to be wished-in-place at a very shallow depth prior to dragging, with the top of the fluke assumed at a depth of $t \approx B/7$ initially (this is because a drag anchor often self-embeds into the seabed due to its own weight). Large soil domain dimensions measuring $150B \times 18B$ have been considered to accommodate the entire anchor travel path within the numerical model. Fig. 3 shows an example of a reconstructed mesh after a drag distance of $0.5B$. The bottom boundary was restrained against both lateral and vertical displacements, whereas only lateral restraint was imposed on the side boundaries. The soil domain was discretized using CPE4 elements (4-node bilinear element), and mesh optimisation was carried out to maintain a balance between computational time and accuracy, where the element sizes varied from $0.02B$ (in close vicinity of the anchor) to B (away from the anchor). The anchor-soil interaction was modelled as either a fully bonded or smooth interface without allowing separation. It should be noted that undrained conditions prevail during installation in the clayey seabed, and thus, not allowing separation at the anchor-soil interface is reasonable to model the suction at the back of the anchor, which is a common practice in the literature (Song et al., 2009; Gaudin et al., 2009).

2.2 Material model

This study focuses on clay seabeds, which are the prevailing case in deep water regions where floating platforms are demanded. The installation of an anchor is typically performed within 3~12 hours. Considering consolidation coefficient of clays lying in the typical range 0.3–5m^2/year, anchor installation is essentially carried out in undrained conditions; and this can be modelled using the Tresca yield criterion in a total stress framework. A Poisson's ratio of 0.49 was assumed to model undrained condition with no volume change and keep numerical stability. To capture the effects of soil remoulding because of the accumulation of plastic shear strain, the Einav & Randolph (2005) model was used in this study:

$$s_{\mathrm{u}} = s_{\mathrm{u0}}\left[\delta_{\mathrm{rem}} + \left(1-\delta_{\mathrm{rem}}\right)e^{-3\xi/\xi_{95}}\right] \tag{1}$$

where s_{u0} is the initial shear strength of the soil, and s_{u} is the remoulded shear strength. Δ_{rem} is the ratio between the completely remoulded s_{u} and intact s_{u0}, i.e., $\delta_{\mathrm{rem}} = 1/S_{\mathrm{t}}$, where S_{t} is the soil sensitivity. S_{t} generally lies in the range of 2–6 for offshore soil conditions (Randolph, 2004). Three different values of S_{t} (= 2, 3, 5) have been investigated here. ξ is the cumulative absolute plastic shear strain, whereas ξ_{95} is the value of ξ corresponding to 95% remoulding. Using T-bar/ball penetrometer tests and laboratory test data, Randolph (2004) and Einav & Randolph (2005) deduced that ξ_{95} typically ranges from 10 to 50. In this study, an intermediate value of ξ_{95} = 20 was chosen. It should be noted that the effects of strain rate on undrained shear strength of soil was not studied; only soil remoulding was modelled to get conservative estimates of anchor performance.

2.3 Incorporation of anchor line mechanics into the numerical model

During installation, the anchor line cuts and slides through the soil, which leads to an inverse catenary profile (see Fig. 2). The anchor line profile evolves during the drag-in process, which influences the magnitude and direction of the line tension acting on the anchor. Vivatrat et al. (1982) expressed the governing differential equations for the embedded portion of the anchor line as:

$$\frac{\mathrm{d}T}{\mathrm{d}s}=F+w\sin\theta;\qquad T\frac{\mathrm{d}\theta}{\mathrm{d}s}=-Q+w\cos\theta \tag{2}$$

where T is the line tension, and ds is the length of an infinitesimal anchor line segment (see the inset in Fig. 2). F and Q are the frictional and normal resistances, respectively, acting on the segment of the line. Θ is the inclination of the segment with respect to the horizontal direction, which varies from θ_a at the padeye to θ_m at the mudline. W is the submerged weight of the line per unit length. Neubecker & Randolph (1995) obtained a closed-form solution to the governing differential equations by neglecting the weight of the anchor line:

$$\frac{T_\mathrm{a}}{1+\mu^2}\left[e^{\mu(\theta_\mathrm{a}-\theta_\mathrm{m})}\left(\cos\theta_\mathrm{m}+\mu\sin\theta_\mathrm{m}\right)-\left(\cos\theta_\mathrm{a}+\mu\sin\theta_\mathrm{a}\right)\right]=\int_0^{z_\mathrm{p}}Q\mathrm{d}z=N_\mathrm{c}E_\mathrm{n}d\left(s_\mathrm{um}+\frac{kz_\mathrm{p}}{2}\right)z_\mathrm{p} \tag{3}$$

where T_a is the line tension at the padeye, and μ is the friction coefficient of the anchor line. N_c, E_n and d are the bearing capacity factor, effective width multiplier and bar diameter of the anchor line, respectively. S_um and k define the undrained shear strength s_u profile of the soil (see Fig. 2), where s_um is the s_u at the mudline, and k is the gradient of s_u along the depth. z_p is the depth of the padeye.

During the anchor installation process, the loading direction of the installation line θ_a continuously changes to be compatible with the loading to the anchor. In the numerical LDFE, precise modelling of this process synchronously with the anchor motion is extremely challenging, and there are two methods available in the literature to account for this. One is to use load control by specifying the loading direction θ_a (Song et al., 2009; Wang et al., 2011; Wang & O'Loughlin, 2014). While this method is accurate in describing the development of the anchor line loading direction, it suffers from a potential numerical convergence problem. The other method is to specify incremental displacement with a fixed pull-out angle in each step of the LDFE analysis (Wang et al., 2011; Tian et al., 2015b; Ghorai & Chatterjee, 2021). However, this method inevitably accumulates errors when the mooring line is not vertical because the padeye is artificially restrained in a specified travel direction during one increment of analysis. This leads to an incorrect estimation of anchor displacement and rotation as shown Fig. 4(a) (note, this error cannot be reduced even by choosing smaller displacement increment and frequently updating θ_a).

This paper adopted a new technique by specifying a small incremental displacement (0.01B) amplitude in the direction of anchor line, but allowing the padeye to travel transversely compatible with the system (see Fig. 4(b)). This is realised by utilising the approach proposed by Tian et al. (2016), wherein a local coordinate system x'-z' was defined with origin at the padeye (see Figs 2–4). The x' axis was oriented along the line direction at the padeye obtained from the last increment analysis, as shown in Fig. 2. In the current incremental step of LDFE analysis, the anchor was displaced by 0.01B along the x' direction while allowing free movement along the z' direction and rotation in the plane. After each incremental step analysis, the depth of the padeye z_p and line direction θ_a were updated. The advantages of this new method are: (a) it is computationally efficient and robust as analyses are performed using displacement-control; (b) it does not restrain anchor movement in a particular direction and remains compatible with the chain movement. A sensitivity study of the values of incremental displacements was performed, and an incremental displacement of 0.01B was proven to be a good balance between accuracy and efficiency. Most of the LDFE analysis cases involved ~6000 incremental steps due to the large dragging distance.

As the anchor line cuts through the soil during anchor penetration, the soil around the line is also likely to undergo remoulding. A parametric study was carried out to investigate the effect of remoulding around the anchor line using the model suggested by Sun et al. (2019), in which the remoulded friction coefficient μ_{res} and normal resistance Q_{res} are based on the initial μ and Q:

$$\mu_{\mathrm{res}} = \frac{8 + 2S_{\mathrm{t}}}{4 + 6S_{\mathrm{t}}}\mu \tag{4}$$

$$Q_{\mathrm{res}} = \left(0.4\delta_{\mathrm{rem}} + 0.6\right)Q \tag{5}$$

where S_{t} is soil sensitivity, and $\delta_{\mathrm{rem}} = 1/S_{\mathrm{t}}$. Because of the extreme challenges involved in large deformation modelling of complicated chain links, Sun et al. (2019) obtained these remoulded coefficients using the Coupled Eulerian-Lagrangian (CEL) technique, which is an explicit dynamic approach requiring careful calibration and user's experience. The remoulded soil resistance around the anchor line was modelled using this approach (and not using RITSS) in this paper since remoulding due to anchor line cutting through soil cannot be modelled using a two-dimensional RITSS approach.

2.4 LDFE modelling procedure and analysis cases

The LDFE modelling procedure is as follows:

1. The finite element mesh is generated at the initial position.

2. A local coordinate system x'-z' is defined, with an origin at the padeye and x' axis inclined at an angle of θ_a with the horizontal (Note: $\theta_a = 0$ for the first step).
3. A small strain analysis is carried out by applying an incremental displacement of $0.01B$ along x' while allowing movement along z' and rotation of the anchor.
4. A new mesh is constructed with the deformed domain obtained from the previous analysis; and stresses, strains and field variables are interpolated from the old mesh to the reconstructed mesh.
5. The values of T_a and z_p are obtained from the previous analysis, and the updated value of θ_a is calculated.
6. Steps 2–5 are repeated until the anchor penetrates to the ultimate embedment depth.

The base case (Case 1) in this paper considers installation of an anchor with $\theta_{fs} = 50°$ in soil with uniform s_u. The anchor, anchor line and soil parameters for this base case are listed in Table 2. In addition, a total of 17 LDFE cases considering variations in computation parameters were conducted, which included studying the effects of various anchor line parameters, soil shear strength profile, padeye location and soil remoulding.

3. The base case

The base case is compared with the well-established plasticity analysis by Cassidy et al. (2012) and analytical solution by Tian et al. (2015a). Cassidy et al. (2012) developed a Fortran program (known as CASPA) based on plasticity theory. Though originally applied to model the keying of suction-embedded plate anchors in Cassidy et al. (2012), the methodology can be reconfigured and equally applied to drag installed anchors (as will be presented here), as it is based on the concept of determining anchor kinematics from yield surface and associated plastic flow rule. The development in line tension at padeye T_a, line inclination at padeye θ_a, embedment depth of fluke centre z_c and fluke orientation α during the drag-in process can be predicted using this method and CASPA program. The analytical solution of Tian et al. (2015a) directly provides the results at the ultimate state. Both studies model the anchor kinematics using the yield envelope (with the equation first adopted by Bransby & O'Neill, 1999) as

$$f = \left(\frac{N_{\mathrm{n}}}{N_{\mathrm{n\,max}}}\right)^{q} + \left[\left(\frac{|N_{\mathrm{m}}|}{N_{\mathrm{m\,max}}}\right)^{m} + \left(\frac{|N_{\mathrm{s}}|}{N_{\mathrm{s\,max}}}\right)^{n}\right]^{1/p} - 1 = 0 \qquad (6)$$

where $N_{\mathrm{n}} = F_{\mathrm{n}}/Bs_{\mathrm{u}}$, $N_{\mathrm{s}} = F_{\mathrm{s}}/Bs_{\mathrm{u}}$ and $N_{\mathrm{m}} = M/B^2s_{\mathrm{u}}$ are nondimensional normal, sliding and moment bearing factors, respectively. F_{n}, F_{s} and M are the resultant normal force, sliding force and rotational moment transferred to the fluke rotation centre from the applied line tension T_{a} and submerged anchor weight W' (see Fig. 2 for illustration of the three components F_{n}, F_{s} and M). $N_{\mathrm{n\,max}}$, $N_{\mathrm{m\,max}}$ and $N_{\mathrm{s\,max}}$ define the size of the yield envelope, whereas m, n, p and q are parameters defining its shape. Typical values of these parameters obtained from previous finite element studies are shown in Table 3. The yield envelope parameters proposed by Elkhatib (2006) were used in the present study to compare the LDFE results.

Fig. 5 shows the LDFE results (variation of T_{a}, θ_{a}, z_{c} and α with drag distance) compared with the analytical solution and CASPA prediction. Fig. 5(a) illustrates the development of line tension, whereas Fig. 5(c) shows the anchor trajectory during installation. With an increase in drag distance, θ_{a} increases gradually, which is accompanied by a reduction in α until both reach a constant value at the ultimate embedment depth (see Figs 5(b) and 5(d)).

Overall agreement between the plasticity approach prediction and the LDFE numerical results is observed (discrepancies less than 1% at the ultimate state), although discrepancies (up to ~ 20% in Fig. 5(c)) are observed at the start of the embedment process (i.e., when embedment is less than ~ $4B$). This discrepancy is due to the yield surface used in CASPA, as the analytical solution is based on a deeply buried mechanism, while the LDFE modelling of this paper can capture the shallow mechanism that is affected by the seabed surface. Fig. 6 shows the contour plots of the incremental soil displacement u_{soil} (obtained from a single step of LDFE) normalised by the incremental padeye displacement u_{padeye}. In the early stage of drag-in, the seabed geometry changes with the formation of a heave on the front side of the fluke. The heave initially grows as the anchor penetrates deeper (compare Figs 6(a) and 6(b)), and the soil flow mechanism extends up to the soil surface. As drag embedment progresses, the mechanism gradually transforms into a localised “flow around” mechanism, as shown in Fig. 6(d); Fig. 6(c) is the intermediate transitional mechanism between shallow and deep mechanisms.

4. Interpretation of the LDFE results

4.1 Effect of fluke-shank angle, θ_{fs}

The three different values of the fluke-shank angle, θ_{fs} =50°, 41° and 32°, recommended for soft, medium and stiff clays by Vryhof (2018), were considered in this study (see Cases 1–3 in Table 2). These correspond to padeye offset ratios $\eta = e_{\mathrm{p}}/e_{\mathrm{n}} = 0.48$, 0.73 and 1.08.

Fig. 7 illustrates the development of T_{a} and z_{c} during installation of the anchor. Table 4 summarises the values of $T_{\mathrm{a}}^{\mathrm{ult}}$, $z_{\mathrm{c}}^{\mathrm{ult}}$, $\theta_{\mathrm{a}}^{\mathrm{ult}}$ and α^{ult} at the ultimate state. T_{a}, z_{c}, θ_{a} and α are significantly lower for anchors with smaller fluke-shank angles θ_{fs}. Fig. 7 also compares the LDFE results with the CASPA predictions for various values of θ_{fs}. An agreement between LDFE and CASPA estimates is seen for $\theta_{\mathrm{fs}} = 50°$, and a significant discrepancy is observed for smaller θ_{fs}. Again, the reason for this discrepancy is that the analytical approaches are based on the yield envelope parameters derived from deep embedment. For θ_{fs} = 32°, z_c^{ult} is ~2.2B, and in such circumstances, the failure mechanism would be different from the deep mechanism (similar to an intermediate mechanism, as shown in Fig. 6(c)).

This is further evidenced from Fig. 8, where Fig. 8(a) shows the load paths in the N_n - N_s - N_m space of LDFE for θ_{fs} = 50°, 41° and 32° (i.e., Cases 1–3), with the yield envelope of Eq. 6 shown. Fig. 8(b) is the projection on the two-dimensional N_n - N_s plane. Each load path starts from the origin (i.e., prior to the tensioning of the anchor line) and approaches the yield envelope. At the ultimate state, the moment bearing factor N_m = 0, since the line tension passes through the anchor rotation centre, and thus, the resulting moment reduces to 0. For θ_{fs} = 32°, the yield envelope size is likely to be smaller than in the deep embedment case. Assuming a smaller yield envelope with $N_{n\ max}$ = 8.5 by keeping other yield envelope parameters unchanged (see Fig. 8), the analytical solution for z_c^{ult} (Tian et al. 2015a) is predicted to be 2.2B, which matches well with the LDFE prediction. This implies that the yield envelope parameters need to be chosen carefully for the accurate estimation of trajectory using the analytical methods, particularly for the cases where the anchor penetrates at a shallow depth.

4.2 Effect of soil strength profile

Deep water seabed strength commonly increases with depth, $s_u = s_{um} + kz$, where k is the shear strength gradient along depth z, and s_{um} is the shear strength at the mudline. kB/s_{um} is a factor representing the heterogeneity of the shear strength profile. As detailed in Table 2, Cases 4–7 were conducted to show the effect of this heterogeneity on the installation response. The LDFE results for s_u = 1 + 1.5z (s_u in kPa, z in m) are shown in Fig. 9. From Fig. 9(b), it can be seen that the anchor penetrates deeper than the uniform s_u profile. This is a result of different soil resistance distribution along the anchor line due to a significant portion of the line interacting with weaker soils located at shallow depths. Consequently, the anchor mobilises a higher holding capacity in a typical normally consolidated strength profile where s_u increases with depth compared to a uniform strength case.

The plasticity and analytical solutions (Cassidy et al., 2012; Tian et al., 2015a) for this case are also shown. It is observed that these solutions overestimate both the penetration depth and the capacity significantly. This is because the plasticity and analytical methods assume s_u as linearly increasing with depth during the entire drag-in process. However, this is not true because the soil from shallow depth can flow with the anchor during drag-in as indicated from the s_u contour in Fig. 10 after a drag distance of 10B. The soft soil dragged along with the anchor can be clearly observed in the LDFE analysis. However, in reality, the anchor-soil interface is not fully rough. The volume of soft soil getting dragged is likely to depend on interface roughness and will be less for a smoother interface. Thus, Cases 4–7 represent the scenario of maximum soft soil being dragged.

Different values of s_um and k were considered, with kB/s_um ranging from 0 to 5, and the values of $z_\mathrm{c}^\mathrm{ult}$ and $T_\mathrm{a}^\mathrm{ult}$ obtained from the LDFE simulations were compared with the analytical solutions. As shown in Fig. 11, $z_\mathrm{c}^\mathrm{ult}{}_\mathrm{LDFE}/z_\mathrm{c}^\mathrm{ult}{}_\mathrm{analytical}$ and $T_\mathrm{a}^\mathrm{ult}{}_\mathrm{LDFE}/T_\mathrm{a}^\mathrm{ult}{}_\mathrm{analytical}$ decrease with kB/s_um. Predictions using the two approaches show up to 11% and 42% differences in $z_\mathrm{c}^\mathrm{ult}$ and $T_\mathrm{a}^\mathrm{ult}$, respectively, as seen when $kB/s_\mathrm{um} = 5$. Again, this highlights the non-conservativeness of the analytical solution by neglecting the dragging of soft soil around the anchor.

4.3 Effect of anchor weight, anchor line parameters and interface roughness

As listed in Table 4, variations in anchor weight, anchor line properties and anchor-soil interface are considered in Cases 8–12. The results are summarised in this section and detailed in Table 4, with no figure presented for brevity.

4.3.1 Anchor weight

A comparison of two anchor weights of 0 and 16.37 kN/m (Cases 1 and 8, see Table 2) shows that the anchor weight does not have any obvious influence on the holding capacity and anchor trajectory. T_a^{ult} and z_c^{ult} for Case 8 with an anchor weight of 16.37 kN/m were 0.1% and 2.2% more than Case 1, respectively. This confirms the conclusions of Murff et al. (2005) and Tian et al. (2015a) that anchor performance is mainly correlated to the geometry and bearing area rather than the weight. However, the majority of the current design practices (NCEL, 1987; API, 2005; Vryhof, 2018) express anchor capacity empirically as a function of anchor weight. The logic behind this is that the weight is related to anchor size. New methods or charts that relate capacity directly to bearing area and geometry are foreseen as an improvement to the current practice.

4.3.2 Anchor line parameters

Dutta & Degenkamp (1989) obtained an anchor line bearing factor N_c of 7.6 from model tests in the laboratory, while DNV (2012) recommends N_c in the range of 9–14. The effective width multipliers E_n are 1 and 2.5 for wire- and chain-type anchor lines, respectively (DNV, 2012). Thus, a lumped value of E_nN_c is considered to range from 7.6 to 35 in the present study. Considering a line diameter d of 0.125 m, three cases of E_nN_cd/B = 0.28, 0.92 and 1.28 were studied, as listed in Table 2 (Cases 1, 9 and 10). The ultimate embedment depth was found to decrease from 11.32B to 3.13B as E_nN_cd/B was increased from 0.11 to 0.51 for θ_{fs} =50° (see Table 4). The results are very sensitive to the value of E_nN_cd chosen, highlighting that the anchor line loading angle θ_a increases significantly with an increase in E_nN_cd, resulting in a lower value of the ultimate embedment depth. Thus, accurate estimation of the anchor line performance is important in predicting the anchor trajectory.

The closed-form solution proposed by Neubecker & Randolph (1995) considers a weightless anchor line (Eq. 2). To investigate the effect of the weight of the line, the governing differential equations defining the anchor line mechanics (Eq. 1) was solved by using the iterative numerical integration scheme proposed by Vivatrat et al. (1982). Case 11 was performed considering a line buoyant weight of 3.3 kN/m as recommended by Vryhof (2018) for a 0.125 m diameter chain. z_c^{ult} was obtained as 18.11 m, which is marginally greater (~6%) than the base case, whereas the T_a^{ult} was nearly unaffected.

4.3.3 Anchor-soil interface roughness

A fully bonded anchor-soil interface was used in the above analyses. Case 12 is conducted to consider a smooth interface (i.e., frictionless tangential behaviour). The results at ultimate depth are shown in Table 4. The anchor capacity at the padeye was reduced by ~48% compared to that at the fully bonded interface. The ultimate embedment depth was observed to be ~17% less than that of the fully bonded interface. This significant reduction in holding capacity and embedment for a smooth interface is not solely due to the sliding friction at the interface. Rather, a higher padeye offset ratio is expected for the smooth interface case to encourage anchors to dive into deeper seabeds because the optimised padeye offset ratio is much larger for low sliding resistance according to Tian et al. (2015a). Thus, the effect of anchor-soil roughness must be considered to optimise the performance of drag anchors.

4.4 Effect of soil remoulding

4.4.1 Soil remoulding around the anchor

The Einav & Randolph (2005) model (Eq. 1) was adopted to account for soil shear strength evolution due to remoulding during the anchor installation process. In the present study, the soil sensitivities S_t were considered to range from 1 to 5 in Cases 1 and 13–15, as listed in Table 2. Fig. 12 shows the development of line tension and the anchor trajectory for various values of soil sensitivity S_t. It is evident that both the installation resistance and embedment depth decreased significantly with an increase in S_t, which led to a loss of holding capacity by 35% ~ 61% and a reduction of embedment depth by 16% ~ 41%. This is because the soil remoulding resulted in smaller line tension T_a compared to the base case, thus leading to a higher value of loading angle θ_a. Fig. 13 shows the normalised shear strength contours (the real time s_u normalised with respect to initial/intact shear strength, s_{u0}) corresponding to a drag distance of $5B$ for $S_t = 2$ and 5. It can be seen that ~$2.5B$ to ~$4B$ width of soil along the anchor trajectory was remoulded for $S_t = 2$–5. Therefore, the anchor tends to end up in a shallower embedment in soils with high sensitivity.

4.4.2 Soil remoulding around both anchor and anchor line

As the anchor line cuts through the soil during the drag-in process, the soil around the line is likely to be remoulded as well. The effects of this remoulding around the line have been incorporated into the LDFE model using the approach proposed by Sun et al. (2019) (see Eqs. 4 and 5). Fig. 14 shows the predicted anchor trajectories considering soil remoulding around both anchor and line (for $S_t = 2$ and 3 in Cases 16 and 17) compared with Cases 13 and 14 (considering remoulding around the anchor only). As seen from Fig. 14, the anchor dives deeper into the soil (by ~ 14%–25% for $S_t = 2$–3) if remoulding around the line is considered. This is because the soil resistance mobilised on the embedded anchor line decreases as S_t increases. Thus, the line angle at the padeye θ_a decreases, which allows the anchor to penetrate deeper resulting in greater ultimate embedment depth (see Table 4).

5. Conclusions

Modelling drag anchor installation is computationally challenging due to the extremely large deformation. This paper carried out a series of LDFE analyses and presented results to examine the installation process. A technique by using local coordinate system (developed by Tian et al., 2016) was implemented that allows the change in loading direction at the padeye to be modelled while maintaining compatibility with the evolution of the anchor line profile. A base case was verified with well-established analytical solutions. A detailed parametric study was then carried out to study the effects of various factors, including anchor, soil and anchor line parameters. The numerical LDFE results confirmed that anchor performance predominantly depends on geometry and bearing area (fluke dimensions, fluke-shank angle) rather than weight, which agrees with previous established studies demonstrating simple correlations between weight and capacity are not appropriate. The major findings from this study can be summarised as:

(1) The plasticity and analytical approaches, based on the yield surface developed from a deeply buried scenario, overpredicts the ultimate embedment depth and the holding capacity when the embedment depth is shallow. Improved yield surface parameters that reflect soil failure mechanism close to the seabed surface are required for plasticity analysis when the anchor penetration is shallow.

(2) LDFE simulations in normally consolidated soils show that a significant volume of soft upper soil may get dragged along with the anchor during installation, leading to shallower embedment and lower capacity. The analytical solutions cannot capture the soil flow during drag-in, and thus, they may not be conservative, with an overprediction of the ultimate embedment and capacity by 11% and 42% in the cases presented.

(3) Soil remoulding around the anchor is found to reduce embedment by 16% ~ 41% and holding capacity at padeye by 35% ~ 61% for S_t = 2–5. Further, remoulding around the

anchor line can cause the anchor to penetrate to a greater depth by ~ 14%–25% for S_t = 2–3. Remoulding has significant implications for offshore engineering practices and should be incorporated in the estimation of drag anchor installation. It should be noted that the strain rate dependency of undrained shear strength has not been modelled.

The anchor was simplified as an equivalent two-dimensional rectangular plate where the influence of shank was accounted for by using an equivalent thickness. Such simplification is necessary because three-dimensional large deformation numerical model with a complex drag anchor geometry is extremely computationally expensive. Future studies on obtaining two-dimensional equivalent plate dimensions (width and thickness) to represent the three-dimensional drag anchor behaviour (for various aspect ratios) are foreseen to provide a good balance between accuracy and computational time. This can be crucial for LDFE analyses as it can make numerical modelling of the commercial drag anchor installation process computationally viable.

Acknowledgements

This research was undertaken with support from an Australian Research Council Discovery Project (DP180103314) and the corresponding author's ARC Future Fellowship (FT200100457).

Data availability statement

Some or all data used are available from the corresponding author by request.

Notation

B	Width of fluke
d	Diameter of anchor line
E	Deformation modulus of soil
E_{n}	Multiplier for obtaining width of anchor line in normal direction
e_{n}	Eccentricity of padeye
e_{p}	Offset of padeye
F, Q	Frictional and normal resistances acting on anchor line
f	Locus of points on yield envelope
k	Shear strength gradient along depth
m, n, p, q	Coefficients defining shape of the yield envelope
N_{c}	Bearing capacity factor of anchor line
N_{n}, N_{s}, N_{m}	Normal, sliding and rotational bearing factor
$N_{\mathrm{n\,max}}$, $N_{\mathrm{s\,max}}$, $N_{\mathrm{m\,max}}$	Normal, sliding and rotational uniaxial bearing capacity factor
Q_{res}	Normal resistance acting on anchor line considering effect of remoulding
S_{t}	Sensitivity of soil
s	Distance measured along anchor line starting from padeye
s_{u}	Undrained shear strength of soil
s_{um}	Undrained shear strength of soil at mudline
s_{u0}	Intact shear strength of soil prior to remoulding
T	Anchor line tension
T_{a}	Anchor line tension at padeye
$T_{\mathrm{a}}^{\mathrm{ult}}$	Ultimate anchor line tension at padeye
t	Fluke thickness

u_{soil}, u_{padeye}	Incremental soil and padeye displacements in one step of LDFE
W'	Submerged weight of anchor
w	Submerged weight of anchor line per unit length
x, z	Horizontal and vertical coordinates
x', z'	Coordinates defined using a local coordinate system with origin at padeye and x' axis tangential to anchor line at padeye
z_{c}	Embedment depth of fluke centre
$z_{\mathrm{c}}^{\mathrm{ult}}$	Ultimate embedment depth of fluke centre
z_{p}	Embedment depth of padeye
δ_{rem}	Ratio of fully remoulded shear strength to intact shear strength
η	Padeye offset ratio
γ'	Submerged unit weight of soil
μ	Friction coefficient of anchor line
μ_{res}	Friction coefficient of anchor line considering effect of remoulding
θ	Inclination of anchor line
θ_{a}	Inclination of anchor line at padeye
$\theta_{\mathrm{a}}^{\mathrm{ult}}$	Ultimate inclination of anchor line at padeye
α	Inclination of fluke
α^{ult}	Ultimate inclination of fluke
θ_{fs}	Angle between fluke and shank
θ_{m}	Inclination of anchor line at mudline
ξ	Accumulated absolute plastic strain
ξ_{95}	Accumulated absolute plastic strain after 95% remoulding

List of abbreviations

LDFE	Large deformation finite element
RITSS	Remeshing and interpolation technique using small strain
SEPLA	Suction embedded plate anchor
VLA	Vertically loaded anchors

References

API (2005). Design and analysis of stationkeeping systems for floating structures. Recommended Practice 2SK, American Petroleum Institute.

Aubeny, C. P. & Chi, C. (2010). Mechanics of drag embedment anchors in a soft seabed. *Journal of Geotechnical and Geoenvironmental Engineering*, 136(1), 57–68. https://doi.org/10.1061/(ASCE)GT.1943-5606.0000198.

Bransby, M. F. & O'Neill, M. (1999). Drag anchor fluke soil interaction in clays. In *Proceedings of the 7th International Symposium on Numerical Models in Geomechanics*, Graz, Austria, pp. 489–494.

Cassidy, M. J., Gaudin, C., Randolph, M. F., Wong, P. C., Wang, D. & Tian, Y. (2012). A plasticity model to assess the keying of plate anchors. *Géotechnique*, 62(9), 825–836. https://doi.org/10.1680/geot.12.OG.009.

Chatterjee, S., Randolph, M. F. & White, D. J. (2012). The effects of penetration rate and strain softening on the vertical penetration resistance of seabed pipelines. *Géotechnique*, 62(7), 573–582. https://doi.org/10.1680/geot.10.P.075.

Chen, Z., Tho, K. K., Leung, C. F. & Chow, Y. K. (2015). Large deformation numerical analysis of plate anchor keying process. In *Frontiers in Offshore Geotechnics III: Proceedings of the 3rd International Symposium on Frontiers in Offshore Geotechnics (ISFOG 2015)*, Oslo, Norway, vol. 1, pp. 845-850: Taylor & Francis Books Ltd.

Dassault Systèmes (2013). Abaqus analysis user's manual. Providence (RI, USA): Simulia Corp.

Dean, E. T. R. (2010). *Offshore geotechnical engineering – principles and practice*. London, UK: Thomas Telford.

DNV (2012). Design and installation of fluke anchors. Recommended Practice DNV RP-E301.

Dou, Y. & Yu, L. (2018). Numerical investigations of the effects of different design angles on the motion behaviour of drag anchors. *Applied Ocean Research*, 76, 199–210. https://doi.org/10.1016/j.apor.2018.05.003.

Dutta, A. & Degenkamp, G. (1989). Behaviour of embedded mooring chains in clay during chain tensioning. In *Proceeding of the 21st Annual Offshore Technology Conference*, Houston, Texas, USA, pp. 551–562. https://doi.org/10.4043/6031-MS.

Einav, I. & Randolph, M. F. (2005). Combining upper bound and strain path methods for evaluating penetration resistance. *International Journal for Numerical Methods in Engineering*, 63(14), 1991–2016. https://doi.org/10.1002/nme.1350.

Elkhatib, S. & Randolph, M. F. (2005). The effect of interface friction on the performance of drag-in plate anchors. In *Proceedings of the 5th International Symposium on Frontiers in Offshore Geotechnics*, Perth, Australia, pp. 171–177.

Elkhatib, S. (2006). The behaviour of drag-in plate anchors in soft cohesive soils. PhD thesis, The University of Western Australia, Crawley, Australia.

Gaudin, C., Tham, K. H. & Ouahsine, S. (2009). Keying of plate anchors in NC clay under inclined loading. *International Journal of Offshore and Polar Engineering*, 19(2), 135–142.

Ghorai, B. & Chatterjee, S. (2021). Effect of keying-induced soil remolding on the ultimate pull-out capacity and embedment loss of strip anchors in clay. *Journal of Geotechnical and Geoenvironmental Engineering*, 147(10), 04021109. https://doi.org/10.1061/(asce)gt.1943-5606.0002623.

Hu, Y. & Randolph, M. F. (1998). A practical numerical approach for large deformation problems in soil. *International Journal for Numerical and Analytical Methods in Geomechanics*, 22(5), 327–350. https://doi.org/10.1002/(SICI)1096-9853(199805)22:5%3C327::AID-NAG920%3E3.0.CO;2-X.

Kong, D., Martin, C. M. & Byrne, B. W. (2017). Modelling large plastic deformations of cohesive soils using sequential limit analysis. *International Journal for Numerical and Analytical Methods in Geomechanics*, 41(18), 1781-1806. https://doi.org/10.1002/nag.2700.

Maitra, S., White, D., Chatterjee, S. & Choudhury, D. (2019). Numerical modelling of seepage and tension beneath plate anchors. *Computers and Geotechnics*, 108, 131–142. https://doi.org/10.1016/j.compgeo.2018.12.022.

Murff, J. D., Randolph, M. F., Elkhatib, S., Kolk, H. J., Ruinen, R. M., Strom, P. J. & Thorne, C. (2005). Vertically loaded plate anchors for deepwater applications. In *Proceedings of the 5th International Symposium on Frontiers in Offshore Geotechnics*, Perth, Australia, pp. 31–48.

NCEL (1987). Drag embedment anchors for navy moorings, Techdata Sheet 83–08R, Naval Civil Engineering Laboratory, Port Hueneme, CA, USA.

Neubecker, S. R. & Randolph, M. F. (1995). Profile and frictional capacity of embedded anchor chains. *Journal of Geotechnical Engineering*, 121(11), 797–803. https://doi.org/10.1061/(ASCE)0733-9410(1995)121:11(797).

Neubecker, S. R. & Randolph, M. F. (1996). The performance of drag anchor and chain systems in cohesive soil. *Marine Georesources & Geotechnology*, 14(2), 77–96. https://doi.org/10.1080/10641199609388305.

O'Neill, M. P., Bransby, M. F. & Randolph, M. F. (2003). Drag anchor fluke soil interaction in clays. *Canadian Geotechnical Journal*, 40(1), 78–94. https://doi.org/10.1139/t02-096.

Randolph, M. F. (2004). Characterization of soft sediments for offshore applications. Keynote Lecture. In *Proceedings of the 2nd International Conference on Characterization*, Porto, Portugal, 1, 209–232.

Randolph, M. F. & Gourvenec, S. (2011). *Offshore geotechnical engineering*. Abingdon, UK: Spon press.

Song, Z., Hu, Y., O’Loughlin, C. & Randolph, M. F. (2009). Loss in anchor embedment during plate anchor keying in clay. *Journal of Geotechnical and Geoenvironmental Engineering*, 135(10), 1475–1485. https://doi.org/10.1061/(ASCE)GT.1943-5606.0000098.

Sun, C., Feng, X., Bransby, M. F., Neubecker, S. R., Randolph, M. F. & Gourvenec, S. (2019). Numerical investigations of the effect of strain softening on the behaviour of embedded mooring chains. *Applied Ocean Research*, 92, 101944. https://doi.org/10.1016/j.apor.2019.101944.

Tian, Y., Cassidy, M. J., Randolph, M. F., Wang, D. & Gaudin, C. (2014a). A simple implementation of RITSS and its application in large deformation analysis. *Computers and Geotechnics*, 56, 160–167. https://doi.org/10.1016/j.compgeo.2013.12.001.

Tian, Y., Cassidy, M. J. & Gaudin, C. (2014b). The influence of padeye offset on plate anchor re-embedding behaviour. *Géotechnique Letters*, 4(1), 39–44. https://doi.org/10.1680/geolett.13.00056.

Tian, Y., Randolph, M. F. & Cassidy, M. J. (2015a). Analytical solution for ultimate embedment depth and potential holding capacity of plate anchors. *Géotechnique*, 65(6), 517–530. https://doi.org/10.1680/geot.14.P.228.

Tian, Y., Gaudin, C., Randolph, M. F. & Cassidy, M. J. (2015b). Influence of padeye offset on bearing capacity of three-dimensional plate anchors. *Canadian Geotechnical Journal*, 52(6), 682–693. https://doi.org/10.1139/cgj-2014-0120.

Tian, Y., Zheng, T., Zhou, T. & Cassidy, M. J. (2016). A new method to investigate the failure envelopes of offshore foundations. In *Proceedings of the 35th International Conference on Ocean, Offshore and Arctic Engineering*, Busan, Korea, OMAE2016–54513. https://doi.org/10.1115/OMAE2016-54513.

Tian, Y., Gaudin, C., Randolph, M. F., Cassidy, M. J. & Peng, B. (2018). Numerical investigation of diving potential and optimization of offshore anchors. *Journal of Geotechnical and Geoenvironmental Engineering*, 144(2), 04017117. https://doi.org/10.1061/(ASCE)GT.1943-5606.0001830.

Tian, Y., Cassidy, M. & Randolph, M. (2020). Optimising anchor design to encourage achieving greater embedment depth and holding capacity. *In Proceedings of the 4th International Symposium on Frontiers in Offshore Geotechnics*, Austin, Texas.

Ullah, S. N., Hou, L. F., Satchithananthan, U., Chen, Z. & Gu, H. (2018). A 3D RITSS approach for total stress and coupled-flow large deformation problems using ABAQUS. *Computers and Geotechnics*, 99, 203-215. https://doi.org/10.1016/j.compgeo.2018.01.018.

Vivatrat, V., Valent, P. J. & Ponterio, A. A. (1982). The influence of chain friction on anchor pile design. In *Proceedings of the 14th Annual Offshore Technology Conference*, Houston, Texas, USA, pp. 153–156. https://doi.org/10.4043/4178-MS.

Vryhof (2018). Vryhof manual: The guide to anchoring. Vryhof Anchors. See http://www.vryhof.com/pdf/anchor_manual.pdf (accessed 01/08/2021).

Wang, D., White, D. J. & Randolph, M. F. (2010). Large deformation finite element analysis of pipe penetration and large-amplitude lateral displacement. *Canadian Geotechnical Journal*, 47(8), 842–856. https://doi.org/10.1139/T09-147.

Wang, D., Hu, Y. & Randolph, M. F. (2011). Keying of rectangular plate anchors in normally consolidated clays. *Journal of Geotechnical and Geoenvironmental Engineering*, 137(12), 1244–1253. https://doi.org/10.1061/(ASCE)GT.1943-5606.0000477.

Wang, D. & O'Loughlin, C. D. (2014). Numerical study of pull-out capacities of dynamically embedded plate anchors. *Canadian Geotechnical Journal*, 51(11), 1263–1272. https://doi.org/10.1139/cgj-2013-0485.

Wang, L. Z., Shen, K. M., Li, L. L. & Guo, Z. (2014). Integrated analysis of drag embedment anchor installation. *Ocean Engineering*, 88, 149–163. https://doi.org/10.1016/j.oceaneng.2014.06.028.

Wang, D., Bienen, B., Nazem, M., Tian, Y., Zheng, J., Pucker, T. & Randolph, M. F. (2015). Large deformation finite element analyses in geotechnical engineering. *Computers and Geotechnics*, 65, 104-114. https://doi.org/10.1016/j.compgeo.2014.12.005.

Wei, Q., Cassidy, M. J., Tian, Y. & Gaudin, C. (2015). Incorporating shank resistance into prediction of the keying behavior of suction embedded plate anchors. *Journal of Geotechnical and Geoenvironmental Engineering*, 141(1), 04014080. https://doi.org/10.1061/(ASCE)GT.1943-5606.0001193.

Yang, M., Murff, J. D. & Aubeny, C. P. (2010). Undrained capacity of plate anchors under general loading. *Journal of Geotechnical and Geoenvironmental Engineering*, 136(10), 1383–1393. https://doi.org/10.1061/(ASCE)GT.1943-5606.0000343.

Yu, L., Liu, J., Kong, X. J. & Hu, Y. (2009). Three-dimensional numerical analysis of the keying of vertically installed plate anchors in clay. *Computers and Geotechnics*, 36(4), 558–567. https://doi.org/10.1016/j.compgeo.2008.10.008.

Zhao, Y. & Liu, H. (2016). Numerical implementation of the installation/mooring line and application to analyzing comprehensive anchor behaviors. *Applied Ocean Research*, 54, 101–114. https://doi.org/10.1016/j.apor.2015.10.007.

List of tables

Figure Captions

Fig. 1 Sketch of drag anchors: (a) Drag embedded anchor with fixed fluke; (b) Vertically loaded anchor

Fig. 2 Problem geometry and notations

Fig. 3 Reconstructed LDFE mesh after anchor drag of distance 0.5*B* (Base case – Case 1)

Fig. 4 Prescribing displacement boundary conditions at padeye using: (a) global coordinate system; (b) local coordinate system

Fig. 5 Benchmarking of the adopted numerical methodology: (a) line tension at padeye; (b) line inclination at padeye; (c) embedment of fluke centre; (d) fluke inclination with horizontal (Base case - Case 1)

Fig. 6 Normalised soil displacement ($u_{\mathrm{soil}}/u_{\mathrm{padeye}}$) contours in soils with uniform s_{u} after drag distances of (a) 0.5*B*; (b) 3*B*; (c) 6*B*; and (d) 12*B* (Base case – Case 1)

Fig. 7 Effect of fluke-shank angle (θ_{fs}) in soils with uniform $\mathrm{s_u}$: (a) line tension at padeye; (b) embedment of fluke centre (Cases 1–3)

Fig. 8 Load paths and yield envelope for θ_{fs} = 50°, 41° and 32°: (a) $N_{\mathrm{n}} – N_{\mathrm{s}} – N_{\mathrm{m}}$ space; (b) $N_{\mathrm{n}} – N_{\mathrm{s}}$ space (Cases 1–3)

Fig. 9 Drag anchor installation response in soils with s_{u} varying along depth: (a) line tension at padeye; (b) normalised embedment of fluke centre (Case 4)

Fig. 10 Shear strength contours corresponding to a drag distance of 10*B* in soils with $s_{\mathrm{u}} = 1 + 1.5z$ (s_{u} in kPa, z in m) for θ_{fs} = 50° (Case 4)

Fig. 11 Comparison between analytically obtained and LDFE-simulated ultimate embedment depth and mobilized line tension at the padeye for various shear strength profiles of soil (θ_{fs} = 50°, Cases 1, 4–7)

Fig. 12 Effect of soil sensitivity on installation response: (a) line tension at padeye; (b) embedment of fluke centre (Cases 1, 13–15)

Fig. 13 Normalised shear strength (s_u/s_{u0}) contours after drag by a distance of 5B considering remoulding in soils: (a) S_t = 2 (Case 14); (b) S_t = 5 (Case 15)

Fig. 14 Comparison of anchor trajectories considering remoulding around anchor line (Cases 16–17) with predicted trajectories ignoring remoulding around the line (Cases 13–14)

Table 1 Overview of various studies on the prediction of drag anchor trajectory and holding capacity

Category	Source	Methodology	Anchor geometry/type
Empirical design charts	NCEL (1987), API (2005), Vryhof (2018)	Design charts and correlations obtained from test data bases	Various types of commercially available drag anchors
Analytical methods	Neubecker & Randolph (1996)	Incremental analysis based on limit equilibrium method	Various types of drag anchors
	O'Neill et al. (2003)	Plasticity approach based on a force-resultant model	Rectangular and wedge-shaped flukes
	Murff et al. (2005)	Analytical approaches based on either limit equilibrium or plasticity analysis	Vertically loaded plate anchors
	Aubeny & Chi (2010)	Plasticity approach based on a force-resultant model	Rectangular fluke and cylindrical shank
	Cassidy et al. (2012)	Plasticity analysis	Originally developed for SEPLA, but shown in this paper to be applicable to other drag installation
	Wang et al. (2014)	Quasi-static analysis considering an integrated system of anchor, line and vessel	Rectangular fluke and cylindrical shank
	Tian et al. (2015a)	Analytical solution for ultimate state based on a force-resultant model	Anchor idealized as a rectangular plate
Advanced numerical modelling	Zhao & Liu (2016), Dou & Yu (2018)	LDFE analysis using coupled Eulerian-Lagrangian technique	Rectangular fluke and rectangular cylindrical shank

Table 2 List of input parameters

Parameters	Base case (Case 1)	Variations		Notes
		Values	Case Number	
Fluke width, B	3.41 m	-	-	
Fluke length, L	3.3 m	-	-	
Fluke thickness, t	0.51 m	-	-	$B/t \approx 7$
Angle between fluke and shank, θ_{fs}	50°	41°, 32°	2, 3	e_p/e_n ranging from 0.48 to 1.08 for shank length of 6.24 m
Shear strength of soil, s_u	20 kPa	$(1 + 1.5z)$ kPa $(5 + 1.5z)$ kPa $(10 + 1.5z)$ kPa $(20 + 1.5z)$ kPa	4 5 6 7	kB/s_{um} varies from 0 to 5. Here, z is depth in m.
Buoyant unit weight of soil, γ'	8 kN/m^3	-	-	
Deformation modulus of soil, E	$500s_{u0}$	-	-	
Poisson's ratio of soil	0.49	-	-	
Buoyant weight of anchor, W'	0	16.37 kN/m	8	
E_nN_cd/B of anchor line	0.92	0.28, 1.28	9, 10	
Buoyant unit weight of anchor line, w	0	3.3 kN/m	11	
Friction coefficient of anchor line, μ	0.3	-	-	
Line angle at mudline, θ_m	0°	-	-	Catenary mooring
Anchor-soil interface roughness	Rough	Smooth	12	
Sensitivity of soil, S_t	1	2, 3, 5	13, 14, 15	For remoulding around anchor
		2, 3	16, 17	For remoulding around anchor line

668 **Table 3** Yield envelope parameters for $B/t = 7$

Parameter	Source			
	O'Neill et al. (2003)	Elkhatib & Randolph (2005)	Elkhatib (2006)	Yang et al. (2010)
$N_{\mathrm{n\,max}}$	11.87	11.93	11.93	11.98
$N_{\mathrm{s\,max}}$	4.29	4.65	4.65	4.39
$N_{\mathrm{m\,max}}$	1.49	1.63	1.63	1.65
m	1.26	1.27	1.28	1.56
n	3.72	3.46	3.44	4.19
p	1.09	1.03	1.27	1.57
q	3.16	3.23	3.93	4.43

669

Table 4 LDFE predicted results for various cases: ultimate values of line tension, fluke embedment, line inclination and fluke inclination

Case Number	Details of variations (cross-referring to Table 2)	Ultimate state					
		Line tension at padeye, T_a^{ult}/L (kN/m)	Embedment of fluke centre, z_c^{ult} (m)	Inclination of line, θ_a^{ult}	Inclination of fluke, α^{ult}	T_a^{ult}/s_uLB	z_c^{ult}/B
1	Base case	661.89	17.06	48.87°	15.65°	9.71	5.00
2	Fluke-shank angle, θ_{fs}	522.55	12.04	44.33°	9.44°	7.66	3.53
3		433.35	7.50	35.89°	6.48°	6.35	2.20
4	s_u profile	956.23	29.43	55.94°	8.75°	-	8.63
5		1009.38	27.28	55.20°	9.06°	-	8.00
6		1140.03	25.94	54.79°	9.39°	-	7.61
7		1412.58	24.15	54.45°	9.77°	-	7.08
8	Buoyant weight of anchor, W'	663.28	17.41	50.76°	13.49°	9.72	5.11
9	E_nN_cd/B	650.50	45.32	48.41°	15.33°	9.54	13.29
10		652.41	13.64	49.83°	14.26°	9.57	4.00
11	Buoyant weight of line, w	659.26	18.11	49.65°	13.90°	9.67	5.31
12	Smooth anchor-soil interface	354.00	14.21	57.79°	6.37°	5.19	4.17
13	Remoulding around anchor (ignoring remoulding around line)	431.55	14.34	53.19°	11.06°	6.33	4.21
14		338.40	11.43	55.21°	13.90°	4.96	3.35
15		256.83	10.08	52.21°	15.46°	3.77	2.96
16	Remoulding around anchor and line	428.28	16.71	53.80°	11.13°	6.28	4.90
17		344.02	15.32	54.18°	11.66°	5.04	4.49

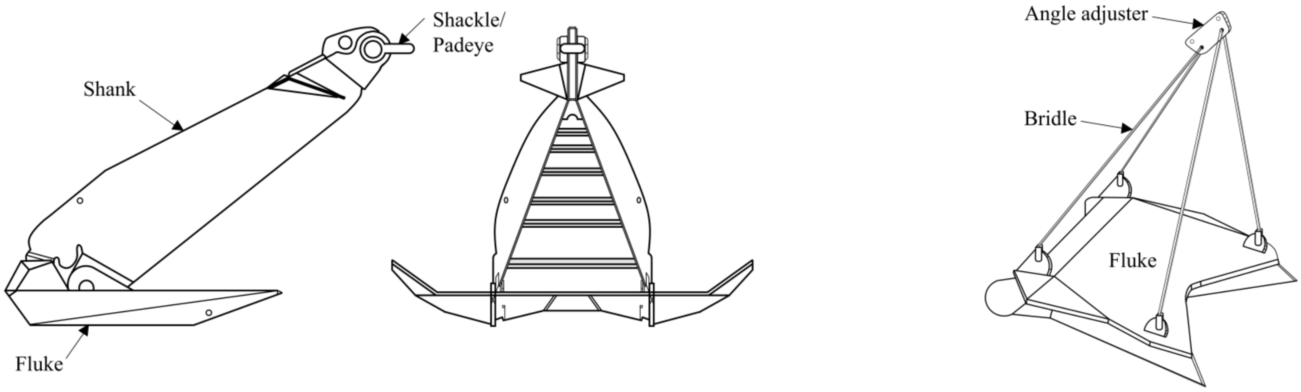

Drag embedded anchor
(a)

Vertically loaded anchor
(b)

Fig. 1 Sketch of drag anchors: (a) Drag embedded anchor with fixed fluke; (b) Vertically loaded anchor

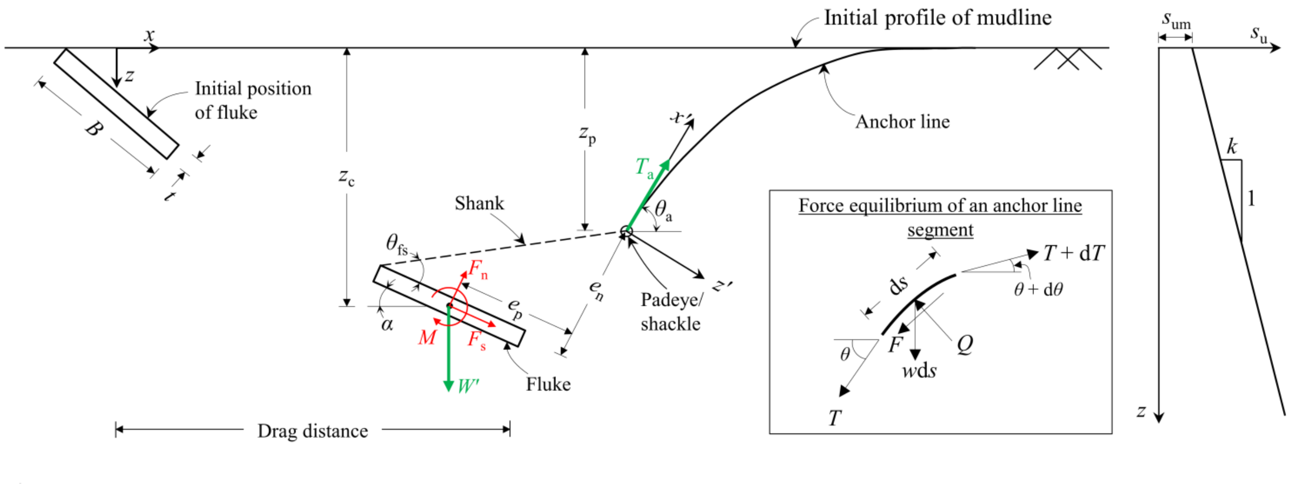

Fig. 2 Problem geometry and notations

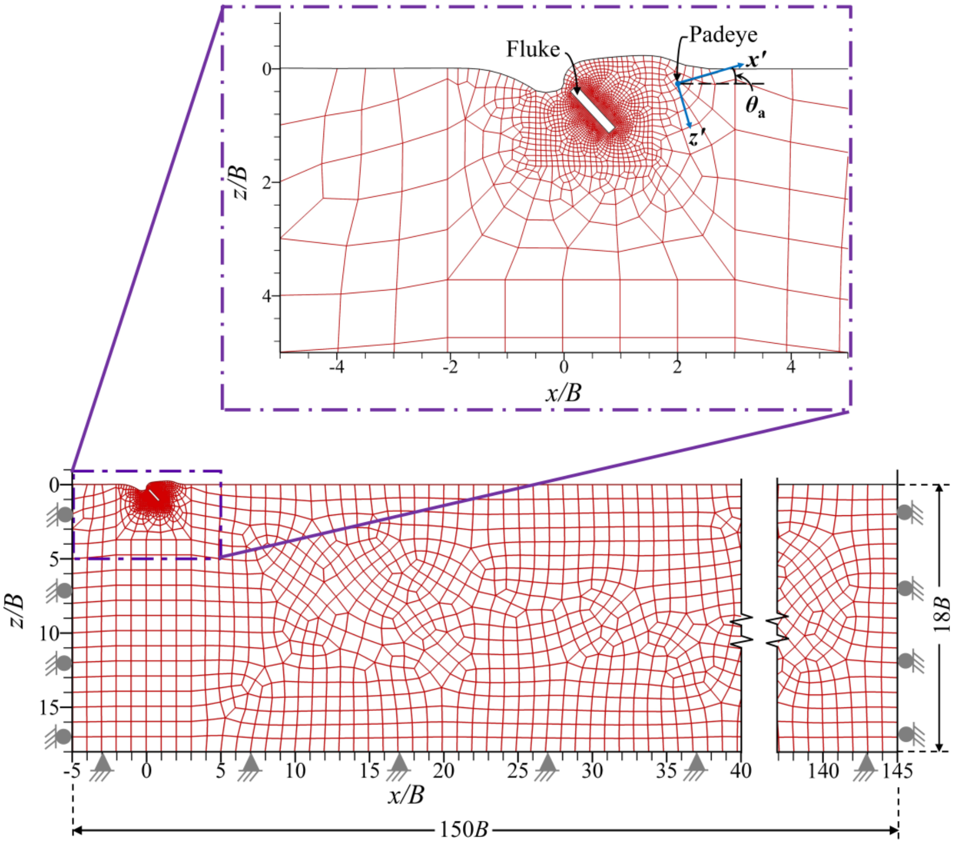

676

677 **Fig. 3** Reconstructed LDFE mesh after anchor drag of distance 0.5*B* (Base case – Case 1)

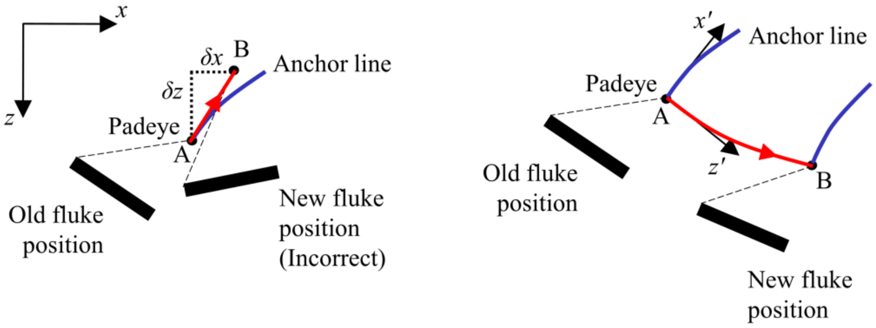

(a) (b)

Fig. 4 Prescribing displacement boundary conditions at padeye using: (a) global coordinate system; (b) local coordinate system

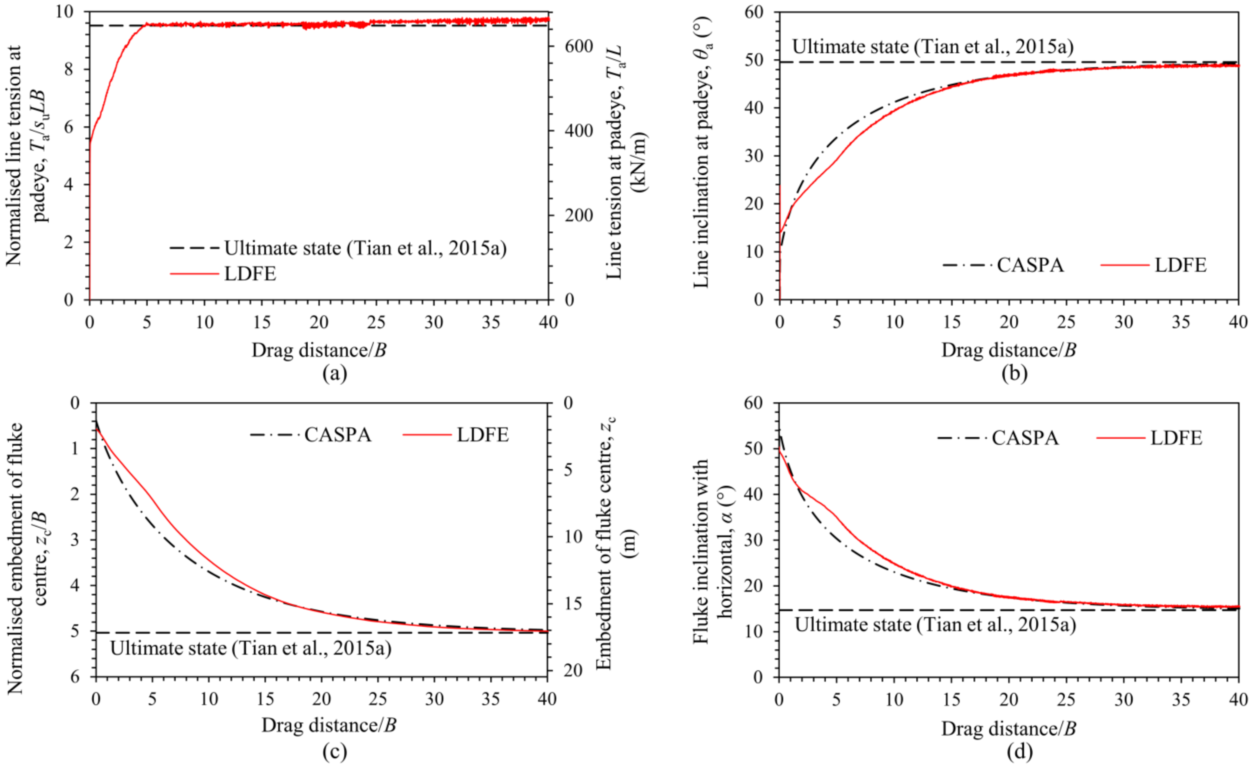

Fig. 5 Benchmarking of the adopted numerical methodology: (a) line tension at padeye; (b) line inclination at padeye; (c) embedment of fluke centre; (d) fluke inclination with horizontal (Base case - Case 1)

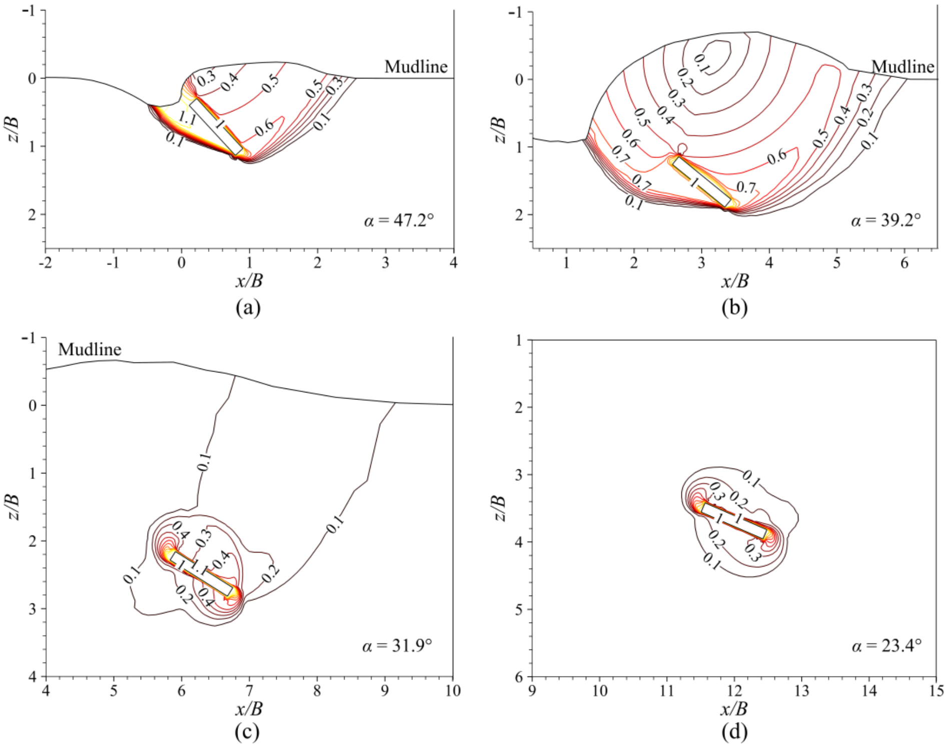

Fig. 6 Normalised soil displacement ($u_{\mathrm{soil}}/u_{\mathrm{padeye}}$) contours in soils with uniform s_u after drag distances of (a) 0.5*B*; (b) 3*B*; (c) 6*B*; and (d) 12*B* (Base case – Case 1)

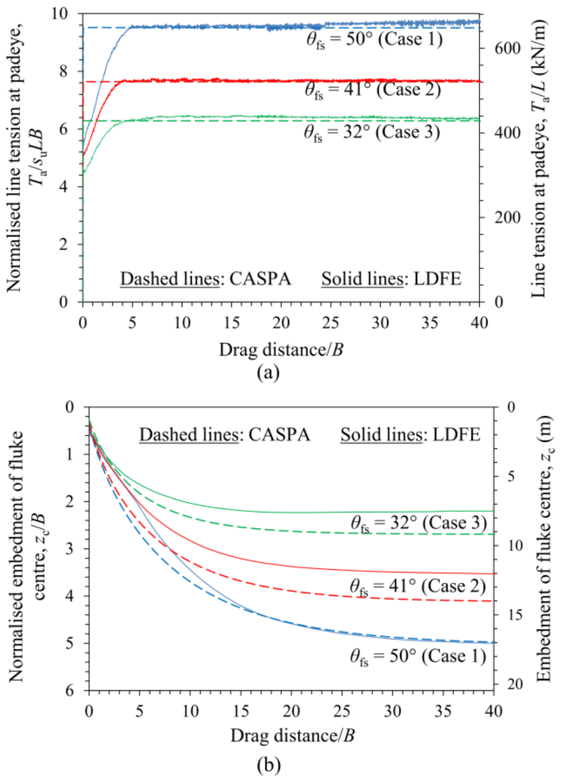

Fig. 7 Effect of fluke-shank angle (θ_{fs}) in soils with uniform s_u: (a) line tension at padeye; (b) embedment of fluke centre (Cases 1–3)

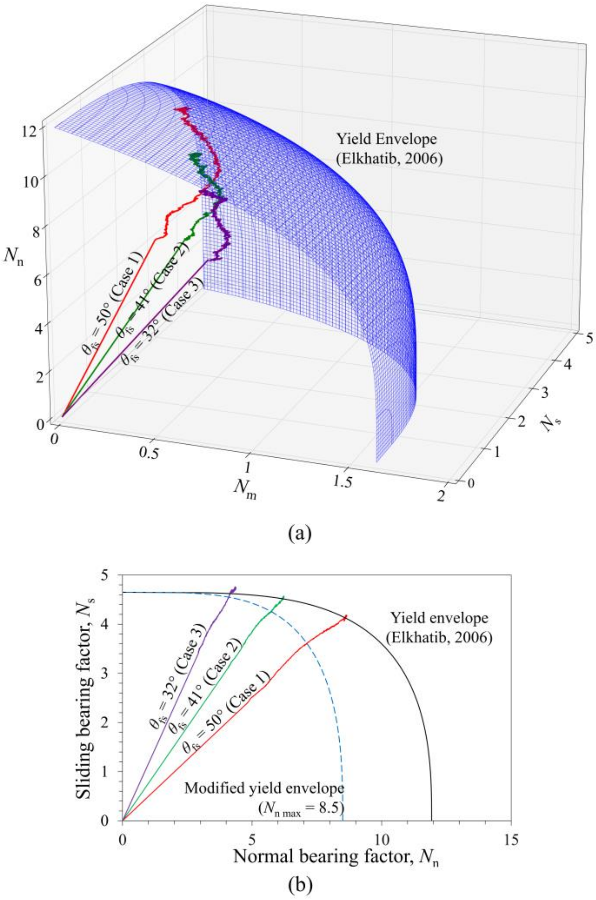

Fig. 8 Load paths and yield envelope for θ_{fs} = 50°, 41° and 32°: (a) N_n – N_s – N_m space; (b) N_n – N_s space (Cases 1–3)

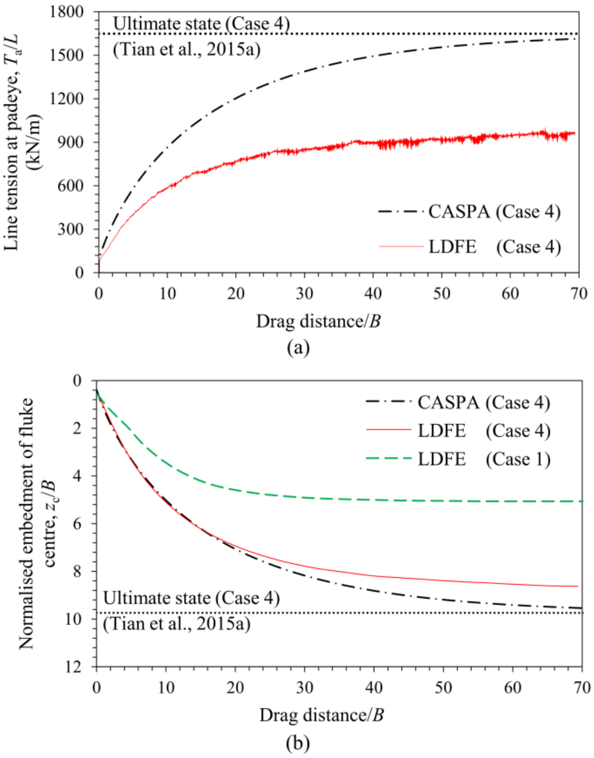

(a)

(b)

Fig. 9 Drag anchor installation response in soils with s_u varying along depth: (a) line tension at padeye; (b) normalised embedment of fluke centre (Case 4)

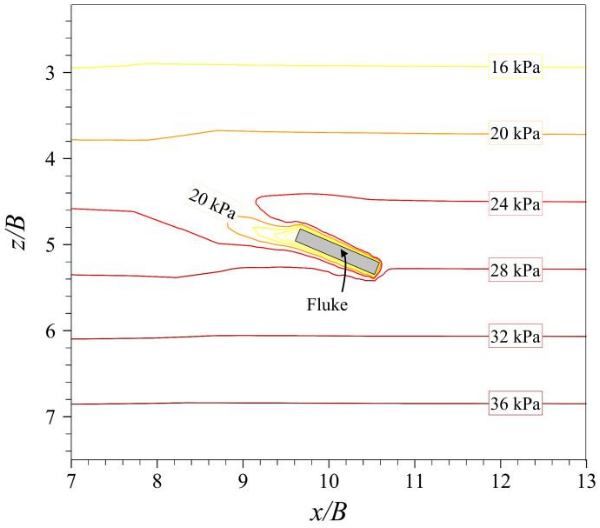

Fig. 10 Shear strength contours corresponding to a drag distance of 10*B* in soils with $s_u = 1 + 1.5z$ (s_u in kPa, z in m) for $\theta_{fs} = 50°$ (Case 4)

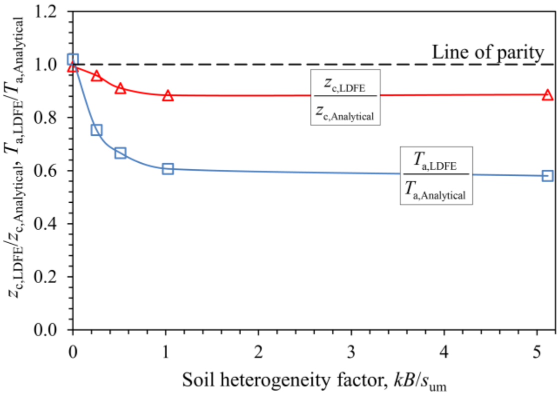

Fig. 11 Comparison between analytically obtained and LDFE-simulated ultimate embedment depth and mobilized line tension at the padeye for various shear strength profiles of soil (θ_{fs} = 50°, Cases 1, 4–7)

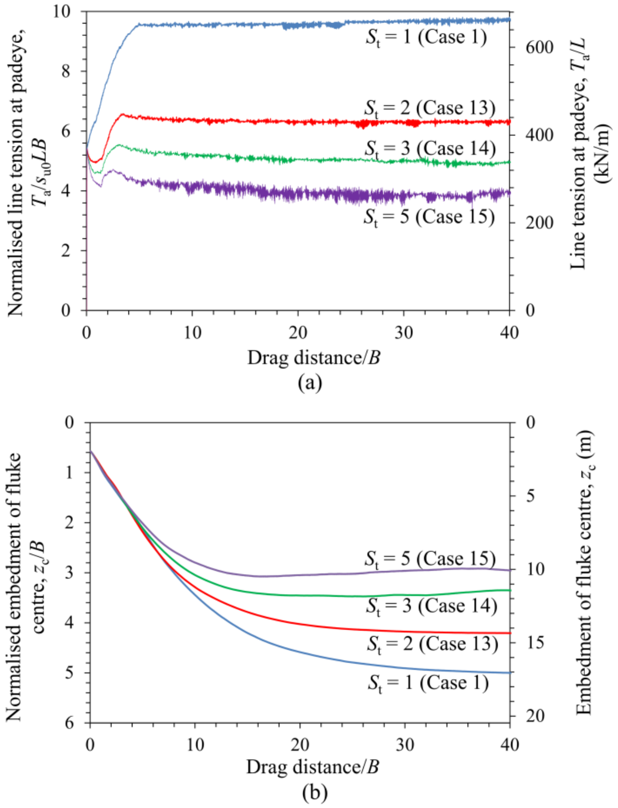

Fig. 12 Effect of soil sensitivity on installation response: (a) line tension at padeye; (b) embedment of anchor (Cases 1, 13–15)

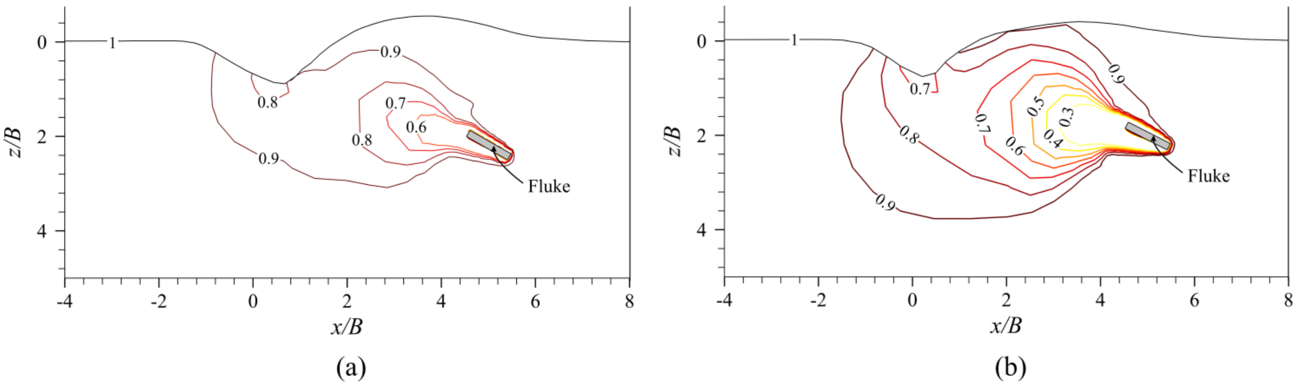

Fig. 13 Normalised shear strength (s_u/s_{u0}) contours after drag by a distance of 5*B* considering remoulding in soils: (a) S_t = 2 (Case 13); (b) S_t = 5 (Case 15)

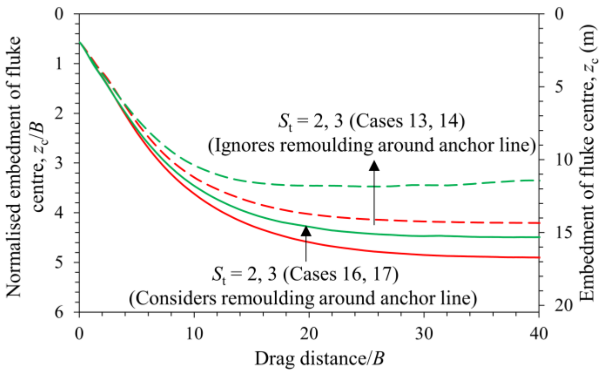

Fig. 14 Comparison of anchor trajectories considering remoulding around anchor line (Cases 16–17) with predicted trajectories ignoring remoulding around the line (Cases 13–14)